J Solid State Eletrochem (2004) 8: 467–473
DOI 10.1007/s10008-004-0500-6

ORIGINAL PAPER

Yi-Shiun Chen · Chi-Chang Hu · Yung-Tai Wu

Capacitive and textural characteristics of manganese oxide prepared by anodic deposition: effects of manganese precursors and oxide thickness

Received: 18 August 2003 / Accepted: 10 December 2003 / Published online: 6 February 2004

Abstract The influence of manganese precursors on the deposition rate of hydrous manganese oxide in the amorphous form (denoted as a-$MnO_x{\cdot}nH_2O$) and the effect of oxide thickness on the electrochemical properties of a-$MnO_x{\cdot}nH_2O$, for application as electrochemical supercapacitors, were systematically investigated in this work. The results showed that $Mn(CH_3COO)_2{\cdot}4H_2O$ is a more promising precursor because of its high deposition rate at much lower potentials in comparison with $MnSO_4{\cdot}5H_2O$, $MnCl_2{\cdot}4H_2O$, and $Mn(NO_3)_2{\cdot}4H_2O$. The capacitive characteristics of a-$MnO_x{\cdot}nH_2O$ were found to be independent of precursors, probably due to the fact that the mean oxidation state of Mn is not significantly affected by changing the anions of manganese precursors (from the XPS results). The capacity of oxide deposits was found to be proportional to the charge density of deposition (i.e., loading) of a-$MnO_x{\cdot}nH_2O$ when it was equal to or less than a critical value (ca. 3.5 C cm^{-2}), while poorer capacitive behavior with a lower capacity was clearly found beyond this critical value. The a-$MnO_x{\cdot}nH_2O$ deposit with 3.5 C cm^{-2}, exhibiting an acceptable capacitive performance, showed the highest capacity of energy storage for supercapacitors.

Keywords Hydrous manganese oxide · Precursors · Thickness · Pseudocapacitance · Supercapacitor

Introduction

Batteries and capacitors are the most common electrical energy storage devices in many applications. The energy density of the former devices is usually much higher than that of the latter, while the power density of capacitors is several orders of most primary energy storage units [1, 2]. Since the demand for power sources delivering significant energy in the high-power or pulse-power form has increased, especially in future electronics, the development of capacitors with high energy densities (i.e., supercapacitors) for these applications has been the interesting subject of much research work [1, 2, 3, 4, 5, 6].

The supercapacitors usually consist of highly porous materials (e.g., activated carbon) with very high specific surface area, or electroactive materials with several oxidation states/structures within the potential window of solvent decomposition [1, 2]. The former devices are also called double-layer capacitors because electric charges are stored within the electrical double layers at the electrode–electrolyte interface [6, 7]. On the other hand, the latter are generally called pseudocapacitors since fast Faradaic reactions at/within the electroactive materials exhibit capacitive-like responses [1, 2, 3, 4, 5]. Because transition-metal oxides (e.g., oxides of Ru, Co, Ni, Mn, V, etc.) and conducting polymers have several oxidation states/structures that lead to redox transitions within the potential region of water decomposition [1, 3, 8, 9, 10, 11, 12, 13], electric energy (i.e., pseudocapacitance) can be stored within these electroactive materials through their highly reversible redox transitions. Since the performance of an electrochemical (EC) supercapacitor is mainly determined by the electrochemical reversibility of superficial electroactive species [1, 5], the electrochemical characteristics of these potential candidates should be examined systematically.

Hydrous manganese oxides prepared by sol–gel-derived, chemical coprecipitation, or electrochemical methods were found to possess capacitive-like behavior [11, 14, 15, 16]. The capacity of a-MnO_2 prepared by a sol–gel-derived method is unacceptable although its specific capacitance is very high [16]. Moreover, pure a-MnO_2 prepared by a chemical coprecipitation method was found to possess poor capacitive characteristics due to the high resistance [15]. Recently, a more convenient

Y.-S. Chen · C.-C. Hu (✉) · Y.-T. Wu
Department of Chemical Engineering,
National Chung Cheng University,
621 Chia-Yi, Taiwan
E-mail: chmhcc@ccu.edu.tw
Tel.: +886-5-2720411
Fax: +886-5-2721206

and acceptable one-step method (i.e., anodic deposition) was proposed to prepare hydrous manganese oxide in the amorphous form (denoted as a-$MnO_x{\cdot}nH_2O$) [11, 17, 18, 19]. Its high electrochemical reversibility and high-power property in the potential window of water decomposition demonstrated an ideal capacitive-like behavior. Moreover, a-$MnO_x{\cdot}nH_2O$, with its nanostructure strongly depending on the anodic deposition modes, is expected to be one of the best potential candidates for application as supercapacitors [18].

More recently, the capacitive behavior of a-$MnO_x{\cdot}nH_2O$ was affected by the introduction of Ni oxide, which exhibited a better capacitive performance in a mixed electrolyte in comparison with Na_2SO_4 [20]. In addition, there may be several Mn precursors suitable for the anodic deposition of a-$MnO_x{\cdot}nH_2O$ although Mn precursors may affect its capacitive performance. Since the energy density of a supercapacitor is greatly enhanced by increasing the loading of electroactive species, the influences of a-$MnO_x{\cdot}nH_2O$ thickness on its capacitive performance are worth investigating The purpose of this work is to investigate the effects of precursors on the deposition rate of a-$MnO_x{\cdot}nH_2O$. In addition, the effects of oxide thickness on the electrochemical characteristics of a-$MnO_x{\cdot}nH_2O$ deposits are also discussed.

Experimental

The a-$MnO_x{\cdot}nH_2O$ deposits were anodically electroplated onto 10×10×3-mm graphite substrates (Nippon Carbon EG-NPL, N.C.K., Japan) under a potentiostatic mode at 1.0 V for variable periods. These substrates were first abraded with ultrafine SiC paper, degreased with acetone and water, then etched in a 0.1 M HCl solution at room temperature (ca. 26 °C) for 10 min, and finally degreased with water in an ultrasonic bath. The exposed geometric area of these pretreated graphite supports is equal to 1 cm^2 while the other surface areas were insulated with poly(tetrafluoroethylene) (PTFE) films. The substrates were placed vertically in the plating solutions during the deposition process. The initial concentration of various Mn precursors in the deposition solutions was 0.1 M. After deposition, the PTFE films were removed from the electrodes and these electrodes were doubly cleaned with cool water flows for 60 s. The electrodes before and after oxide growth were dried in a vacuum oven at room temperature overnight. In order to avoid the interference due to the change in the Mn^{2+} concentration on the deposition rate, every electrode was plated in a freshly prepared solution.

The average oxide loading of hydrous oxide-coated electrodes was obtained from the weight difference of the dried electrodes without PTFE coatings before and after deposition, using a microbalance with a precision of 10 μg (Sartorius BP 211D, Germany). The X-ray diffraction patterns were obtained from X-ray diffraction analysis (XRD: Rigaku X-ray diffractometer using a Cu target) at an angle speed of 4° (2θ) min^{-1}. X-ray photoelectron spectroscopic (XPS) measurements were performed with an ESCA 210 (VG Scientific Ltd.) spectrometer. XPS spectra employed MgKα ($h\nu = 1253.6$ eV) irradiation as the photosource, with a primary voltage of 12 kV and an emission current of 17 mA. The analysis chamber pressure during scans was approximately 10^{-10} mbar.

Electrochemical measurements for a-$MnO_x{\cdot}nH_2O$ deposits were performed by means of electrochemical analyzer systems, CHI 633A (CH Instruments, USA). All experiments were carried out in a three-compartment cell. An Ag/AgCl electrode (Argenthal, 3 M KCl, 0.207 V vs. SHE at 25 °C) was used as the reference and a piece of platinum gauze with an exposed area equal to 4 cm^2 was employed as the counter electrode. A Luggin capillary, whose tip was set at a distance of 1–2 mm from the surface of the working electrode, was used to minimize errors due to iR drop in the electrolytes.

All solutions used in this work were prepared with 18 MΩ cm water produced by a reagent water system (Milli-Q SP, Japan), and all reagents not otherwise specified in this work were Merck, GR. The solutions used for anodic deposition and the electrolytes employed for electrochemical characterization were degassed with purified nitrogen before electrochemical measurements and nitrogen was passed over the solutions during the measurements. The solution temperature was maintained at 25 °C by means of a water thermostat (Haake DC3 and K20).

Results and discussion

Effects of precursors on the deposition and capacitive behavior of a-$MnO_x{\cdot}nH_2O$

Linear sweep voltammograms (LSV) measured in various precursor solutions are used to obtain the effects of precursors on the deposition behavior of a-$MnO_x{\cdot}nH_2O$. Typical results measured at 2 mV s^{-1} in 0.1 M $MnSO_4{\cdot}5H_2O$, $MnCl_2{\cdot}4H_2O$, $Mn(NO_3)_2{\cdot}4H_2O$, and $Mn(CH_3COO)_2{\cdot}4H_2O$ are shown as curves 1–4, respectively, in Fig. 1. On curves 1–3, anodic currents become visible around 0.8 V, indicating that the oxidation of $MnSO_4{\cdot}5H_2O$, $MnCl_2{\cdot}4H_2O$, and $Mn(NO_3)_2{\cdot}4H_2O$ occurs significantly at this potential, at which they are converted to a-$MnO_x{\cdot}nH_2O$. The peak currents (i_P) on these curves are similar and close to 9.5 mA cm^{-2} with their peak potentials (E_P) at ca. 1.2 V. Based on the above LSV results, the anodic deposition behavior of a-$MnO_x{\cdot}nH_2O$ from $MnSO_4{\cdot}5H_2O$, $MnCl_2{\cdot}4H_2O$, and $Mn(NO_3)_2{\cdot}4H_2O$ is very similar. This phenomenon suggests that the mechanisms of a-$MnO_x{\cdot}nH_2O$ deposition from these precursors should be identical. If this is the case, a-$MnO_x{\cdot}nH_2O$ prepared from these three

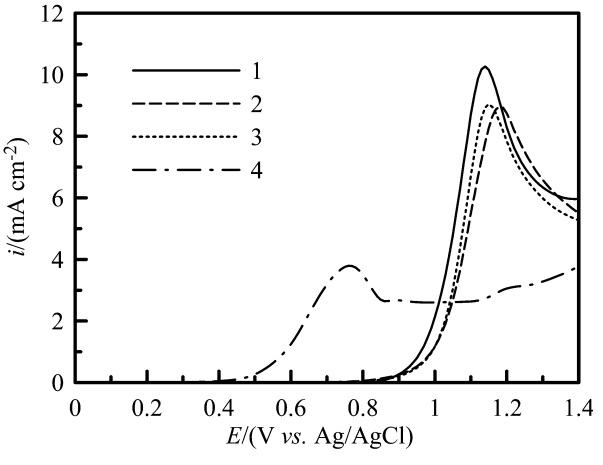

Fig. 1 LSV curves measured at 2 mV s^{-1} in 0.1 M *1* $MnSO_4{\cdot}5H_2O$, *2* $MnCl_2{\cdot}4H_2O$, *3* $Mn(NO_3)_2{\cdot}4H_2O$, and *4* $Mn(CH_3COO)_2{\cdot}4H_2O$

precursors will have very similar capacitive characteristics with a very close mean oxidation state of Mn when the deposition conditions (e.g., deposition mode, pH, temperature, deposition charges, etc.) are the same. The small differences in i_P and E_P on curves 1–3 probably result from the minor influence of anions, since initial pH values of the deposition solutions were found to insignificantly influence the deposition behavior of a-$MnO_x{\cdot}nH_2O$ from $MnSO_4{\cdot}5H_2O$ at pH≥3.0 [11].

On curve 4, the deposition of a-$MnO_x{\cdot}nH_2O$ from the acetate precursor commences at ca. 0.4 V and i_P reaches ca. 4 mA cm^{-2} at ca. 0.75 V and remains a limiting current of ca. 3 mA cm^{-2} at potentials above 0.85 V. The former result indicates that $Mn(CH_3COO)_2{\cdot}4H_2O$ can be decomposed at a much lower potential. The latter result indicates a high deposition rate under diffusion control from 0.75 to 1.3 V, revealing that a-$MnO_x{\cdot}nH_2O$ can be electrochemically deposited onto the substrate in a wide potential region. Thus, the charge of oxide deposition integrated from curve 4 (i.e., $Mn(CH_3COO)_2{\cdot}4H_2O$) is far more than that from curves 1–3. On the other hand, the smaller peak current on curve 4, compared with that on curves 1–3, implies that the deposition mechanism (e.g., elementary steps of a-$MnO_x{\cdot}nH_2O$ deposition, rate-determining step, electron transfer number, etc.) and/or the final oxidation state of a-$MnO_x{\cdot}nH_2O$ from the acetate precursor may be different from those from the other precursors.

In order to gain a further understanding of the reaction mechanisms and the influences of precursors, Tafel plots (i.e., log(i)–E curves) for the deposition of a-$MnO_x{\cdot}nH_2O$ in the plating solutions with 0.1 M $MnSO_4{\cdot}5H_2O$, $MnCl_2{\cdot}4H_2O$, $Mn(NO_3)_2{\cdot}4H_2O$, and $Mn(CH_3COO)_2{\cdot}4H_2O$ were compared and their results measured at 0.5 mV s^{-1} are shown in Fig. 2 as curves 1–4, respectively. Note that the i–E curves of a-$MnO_x{\cdot}nH_2O$ deposition from $MnSO_4{\cdot}5H_2O$, $MnCl_2{\cdot}4H_2O$, and $Mn(NO_3)_2{\cdot}4H_2O$ approximately follow the same trace in the same potential region. This result supports the statement that the mechanisms of a-$MnO_x{\cdot}nH_2O$ deposition from these three precursors are identical. The Tafel slope of these plots is equal to 132 ± 5 mV decade^{-1}, indicating that the electron transfer number in the rate-determining step should be 1 (i.e., Tafel slope = $2.303RT/\alpha nF$; $n = 1$, $\alpha = 0.45$). On curve 4, the Tafel slope is about 160 mV decade^{-1}, indicating that the deposition mechanism of a-$MnO_x{\cdot}nH_2O$ from the acetate precursor is different from that deposited from the other precursors.

The voltammetric behavior of a-$MnO_x{\cdot}nH_2O$ deposits prepared from 0.1 M $MnSO_4{\cdot}5H_2O$, $MnCl_2{\cdot}4H_2O$, $Mn(NO_3)_2{\cdot}4H_2O$, and $Mn(CH_3COO)_2{\cdot}4H_2O$ under a potentiostatic mode at 1.0 V with the same deposition charge is systematically compared to obtain the influences of precursors on the electrochemical characteristics of a-$MnO_x{\cdot}nH_2O$. Typical cyclic voltammograms (CVs) of these oxide-coated electrodes with a deposition charge density of 1.6 C cm^{-2} measured at 25 mV s^{-1} in 0.1 M Na_2SO_4 are shown as curves 1–4, respectively, in Fig. 3. Note that the loading of a-$MnO_x{\cdot}nH_2O$ deposited from 0.1 M $MnSO_4{\cdot}5H_2O$, $MnCl_2{\cdot}4H_2O$, and $Mn(NO_3)_2{\cdot}4H_2O$ is approximately the same (i.e., 0.98, 1.02, and 1.02 mg cm^{-2}, respectively). However, the deposit loading of a-$MnO_x{\cdot}nH_2O$ plated from $Mn(CH_3COO)_2{\cdot}4H_2O$ is 1.11 mg cm^{-2}, indicating a higher efficiency of deposition. Therefore, the voltammetric charge surrounded by curve 4 is significantly higher than those surrounded by curves 1–3. Also note that the i–E responses measured in Na_2SO_4 for a-$MnO_x{\cdot}nH_2O$ deposited from sulfate, chloride, and nitrate precursors are very similar, implying the similar electrochemical properties. In addition, the CV diagrams of these a-$MnO_x{\cdot}nH_2O$ deposits show a typically rectangular shape, indicating the ideal capacitive behavior.

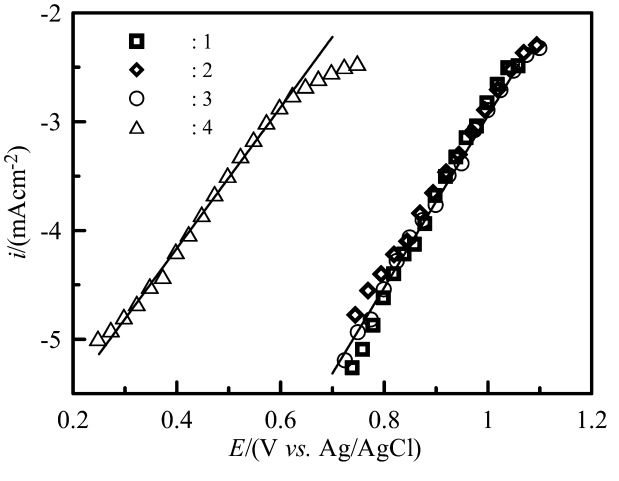

Fig. 2 log(i)–E plots for the deposition of a-$MnO_x{\cdot}nH_2O$ in 0.1 M *1* $MnSO_4{\cdot}5H_2O$, *2* $MnCl_2{\cdot}4H_2O$, *3* $Mn(NO_3)_2{\cdot}4H_2O$, and *4* $Mn(CH_3COO)_2{\cdot}4H_2O$ at 0.5 mV s^{-1}

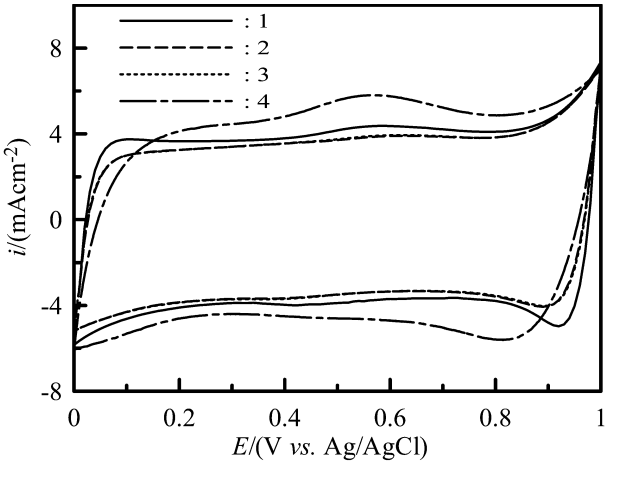

Fig. 3 CV curves of a-$MnO_x{\cdot}nH_2O$ with a deposition charge density of 1.6 C cm^{-2} prepared from 0.1 M *1* $MnSO_4{\cdot}5H_2O$, *2* $MnCl_2{\cdot}4H_2O$, *3* $Mn(NO_3)_2{\cdot}4H_2O$, and *4* $Mn(CH_3COO)_2{\cdot}4H_2O$ measured in 0.1 M Na_2SO_4 at 25 mV s^{-1}

This result further supports the statement that a-$MnO_x{\cdot}nH_2O$ prepared from the above three precursors have very similar capacitive characteristics with a very close mean oxidation state when the deposition conditions are the same. On the other hand, the voltammetric behavior of a-$MnO_x{\cdot}nH_2O$ prepared from acetates also shows capacitive-like characteristics, which is very similar in shape to that of curves 1–3. The above result indicates that the capacitive characteristics of a-$MnO_x{\cdot}nH_2O$ are not significantly affected by changing the anions of the precursors, although the deposition mechanism of a-$MnO_x{\cdot}nH_2O$ is indeed affected by changing the precursors. Accordingly, the structure and the mean oxidation state of a-$MnO_x{\cdot}nH_2O$ deposited from $Mn(CH_3COO)_2{\cdot}4H_2O$ should be very similar to those of a-$MnO_x{\cdot}nH_2O$ prepared from the other three precursors, which is not predictable from its deposition behavior. On the other hand, the capacitive behavior of all a-$MnO_x{\cdot}nH_2O$ deposits is excellent, revealing their potential for application to electrochemical supercapacitors.

From the above results and discussion, the structure and mean oxidation state of a-$MnO_x{\cdot}nH_2O$ prepared from $Mn(CH_3COO)_2{\cdot}4H_2O$ should be very similar to those prepared from the other three precursors. This statement is supported by the fact that all a-$MnO_x{\cdot}nH_2O$ deposits fabricated from different precursors show the amorphous structure in their XRD patterns (not shown here). In addition, XPS spectra of Mn for various a-$MnO_x{\cdot}nH_2O$ deposits prepared from different precursors were compared to gain the reconstructive information of a-$MnO_x{\cdot}nH_2O$ (see Fig. 4). In Fig. 4a–c the broad peaks of Mn $2p_{3/2}$ are centered at ca. 642.5 eV for a-$MnO_x{\cdot}nH_2O$ deposits plated from $MnSO_4{\cdot}5H_2O$, $MnCl_2{\cdot}4H_2O$, and $Mn(CH_3COO)_2{\cdot}4H_2O$. This result indicates that the mean oxidation state of Mn on these deposits should be very similar. In addition, the broad peak of Mn $2p_{3/2}$ indicates that a-$MnO_x{\cdot}nH_2O$ should consist of mixed oxy–hydroxyl–manganese species at various oxidation states. Therefore, the amorphous manganese oxide prepared in this work is considered to exist in a nonstoichiometric structure rather than a well-defined oxidation state, which has also been found previously [17, 18]. This statement is also supported by the peak separation of the multiplet splitting of Mn 3s peaks, since it can be used to determine the oxidation state of Mn [21, 22]. The peak separation of the multiplet splitting of Mn 3s peaks was equal to 4.90, 4.93, and 4.86 eV when a-$MnO_x{\cdot}nH_2O$ was deposited at 1.0 V for 1.6 C cm^{-2} from $MnSO_4{\cdot}5H_2O$, $MnCl_2{\cdot}4H_2O$, and $Mn(CH_3COO)_2{\cdot}4H_2O$, respectively. These results reveal that the pristine a-$MnO_x{\cdot}nH_2O$ deposits should be an oxide aggregation consisting of Mn^{4+} and Mn^{3+} species. Hence, the nonstoichiometric a-$MnO_x{\cdot}nH_2O$ deposits probably result in their amorphous nature. From all the above results and discussion, the electrochemical properties of various a-$MnO_x{\cdot}nH_2O$ deposits are not significantly affected by changing the anion of Mn precursors because of their amorphous structure and a very close mean oxidation state of Mn.

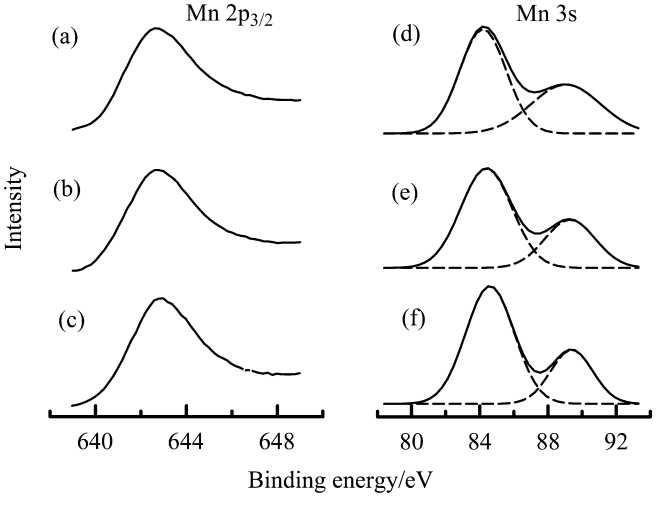

Fig. 4a–f XPS spectra of **a–c** Mn $2p_{3/2}$ and **d–f** Mn 3 s for a-$MnO_x{\cdot}nH_2O$ with a deposition charge density of 1.6 C cm^{-2} prepared from 0.1 M **a**, **d** $MnSO_4{\cdot}5H_2O$, **b**, **e** $MnCl_2{\cdot}4H_2O$, and **c**, **f** $Mn(CH_3COO)_2{\cdot}4H_2O$

Effects of oxide thickness

From the results and discussion in the previous section, the deposition of a-$MnO_x{\cdot}nH_2O$ from $Mn(CH_3COO)_2{\cdot}4H_2O$ is easier than that from the other three precursors and the capacitive performance of a-$MnO_x{\cdot}nH_2O$ is insignificantly affected by changing the anion of the precursors. Accordingly, $Mn(CH_3COO)_2{\cdot}4H_2O$ is indeed a more promising precursor for fabricating the electroactive materials of a-$MnO_x{\cdot}nH_2O$-based supercapacitors by the anodic deposition method. On the basis of the above opinion, $Mn(CH_3COO)_2{\cdot}4H_2O$ was employed as the model precursor for investigating the effect of oxide thickness on the electrochemical properties of a-$MnO_x{\cdot}nH_2O$. The oxide thickness may influence the electrochemical characteristics of a-$MnO_x{\cdot}nH_2O$ significantly because of the poor conductivity of MnO_2 [15]. In addition, the proton diffusion path should become longer with the oxide thickness since a-$MnO_x{\cdot}nH_2O$ will exchange protons with the electrolyte solution during the redox transitions [11, 17]:

$$MnO_a(OH)_b + \delta H^+ + \delta e^- = MnO_{a-\delta}(OH)_{b+\delta} \qquad (1)$$

where $MnO_a(OH)_b$ and $MnO_{a-\delta}(OH)_{b+\delta}$ indicate interfacial oxy–hydroxyl–Mn species at higher and lower oxidation states, respectively.

Various deposits plated by the potentiostatic mode at 1.0 V from a 0.1 M $Mn(CH_3COO)_2{\cdot}4H_2O$ solution with the deposition time of 5, 10, 15, 20, 30, and 40 min were employed to investigate the effect of oxide thickness on the electrochemical characteristics of a-$MnO_x{\cdot}nH_2O$. In addition, these oxide deposits were respectively denoted as a-$MnO_x{\cdot}nH_2O$-5, a-$MnO_x{\cdot}nH_2O$-10, a-$MnO_x{\cdot}nH_2O$-15,

a-$MnO_x{\cdot}nH_2O$-20, a-$MnO_x{\cdot}nH_2O$-30, and a-$MnO_x{\cdot}nH_2O$-40. Typical CV results measured in 0.1 M Na_2SO_4 at 25 mV s^{-1} are shown in Fig. 5. Note that the electrochemical responses of a-$MnO_x{\cdot}nH_2O$-5, a-$MnO_x{\cdot}nH_2O$-10, and a-$MnO_x{\cdot}nH_2O$-15 (see curves 1–3) show rectangular-like and symmetric behavior. In addition, the voltammetric currents on these curves increase on prolonging the deposition time, revealing the fact that electric energy stored within these deposits is mainly contributed by the redox transitions of a-$MnO_x{\cdot}nH_2O$ (i.e., pseudocapacitance). All these results reveal the ideality of capacitive performance for a-$MnO_x{\cdot}nH_2O$ deposited by electrochemical modes.

However, the above phenomena are not found for curves 4–6, demonstrating the influence of oxide thickness. The voltammetric responses of a-$MnO_x{\cdot}nH_2O$-20 (see curve 4) are rugby ball-like rather than rectangular-like, indicating a decay in the electrochemical reversibility. Note that the voltammetric charges surrounded by curves 5 and 6, corresponding to a-$MnO_x{\cdot}nH_2O$-30 and a-$MnO_x{\cdot}nH_2O$-40, are unexpectedly smaller than that corresponding to a-$MnO_x{\cdot}nH_2O$-20. In addition, the heavier the loading of a-$MnO_x{\cdot}nH_2O$, the smaller voltammetric charge the deposit has. Based on this result, there should exist a limitation on the capacity of a-$MnO_x{\cdot}nH_2O$ deposits for the application of supercapacitors. The decay in the electrochemical reversibility of a-$MnO_x{\cdot}nH_2O$ on prolonging the deposition time probably results from the increase in ESR (equivalent series resistance) for a heavier deposit because of the poor conductivity of amorphous MnO_2 [15] and/or the significance of the proton diffusion barrier on this deposit.

From a comparison of all curves in Fig. 5, the electrochemical reversibility seems to be gradually changed on increasing the loading of a-$MnO_x{\cdot}nH_2O$. This statement is supported from an examination of the dependence of deposition charge density, loading, and capacitance of corresponding a-$MnO_x{\cdot}nH_2O$ deposits on the deposition times, shown as curves 1–3 in Fig. 6, respectively. The capacitance of an electrode can be estimated from the voltammetric charge surrounded by the CV curves according to Eq. 2:

$$C = \frac{q}{2\Delta V} \tag{2}$$

where q and ΔV are the voltammetric charges surrounded by the CV curve and the potential range of CV (i.e., 1.0 V), respectively. Data shown as curve 3 in Fig. 6 are the typical results deduced from the voltammetric curves shown in Fig. 5 on the basis of Eq. 2.

Note that the charge density of deposition and loading is directly proportional to the deposition time from curves 1 and 2. This result indicates that a-$MnO_x{\cdot}nH_2O$ can be easily deposited by electrochemical methods from $Mn(CH_3COO)_2{\cdot}4H_2O$. On curve 3, the capacitance of a-$MnO_x{\cdot}nH_2O$ is rapidly increased on prolonging the deposition time when it is equal to or less than 15 min, although the electrochemical reversibility of a-$MnO_x{\cdot}nH_2O$-15 seems to be not as good as that of a-$MnO_x{\cdot}nH_2O$-5. Hence, the energy stored within a-$MnO_x{\cdot}nH_2O$ increases with the oxide loading under the above conditions. On the other hand, an opposite phenomenon is clearly found when the deposition time is equal to or longer than 20 min. Based on the results and discussion for Figs. 5 and 6, the deposit with a maximum capacity and acceptable characteristics for application as supercapacitors should be located in the deposition time between 15 and 20 min (i.e., the charge density of deposition between 2.72 and 3.68 C cm^{-2}).

Based on the above inference, the a-$MnO_x{\cdot}nH_2O$ deposits with a deposition charge density of 3.0 and 3.5 C cm^{-2} (respectively denoted as a-$MnO_x{\cdot}nH_2O$-3C and a-$MnO_x{\cdot}nH_2O$-3.5C) were examined in this work. Typical CV diagrams of a-$MnO_x{\cdot}nH_2O$-3C and a-$MnO_x{\cdot}nH_2O$-3.5C measured in 0.1 M Na_2SO_4 at 25 mV s^{-1} are shown in Fig. 7 as curves 1 and 2, respectively. Note that the difference in the voltammetric

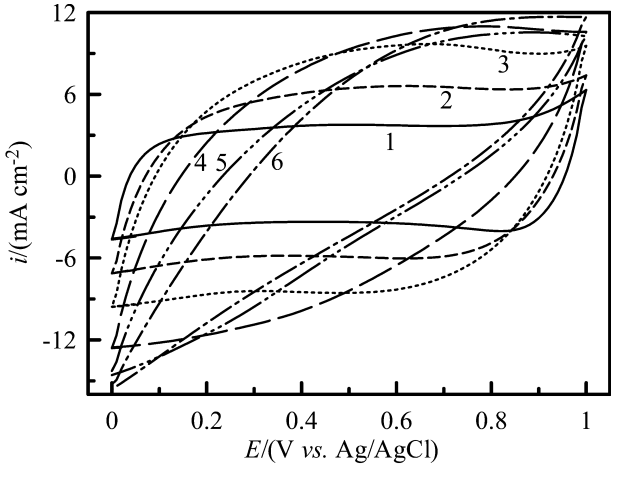

Fig. 5 CV curves of a-$MnO_x{\cdot}nH_2O$ measured in 0.1 M Na_2SO_4 at 25 mV s^{-1}. All deposits were prepared from $Mn(CH_3COO)_2{\cdot}4H_2O$ in a potentiostatic mode at 1.0 V for *1* 5, *2* 10, *3* 15, *4* 20, *5* 30, and *6* 40 min

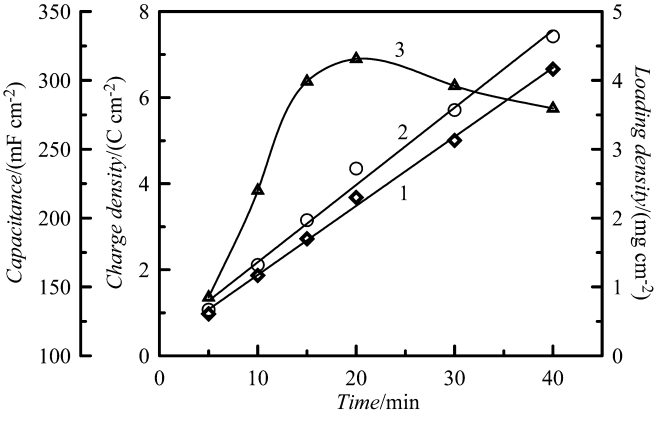

Fig. 6 The dependence of *1* deposition charge density, *2* loading, and *3* capacitance of a-$MnO_x{\cdot}nH_2O$ deposits on the deposition time

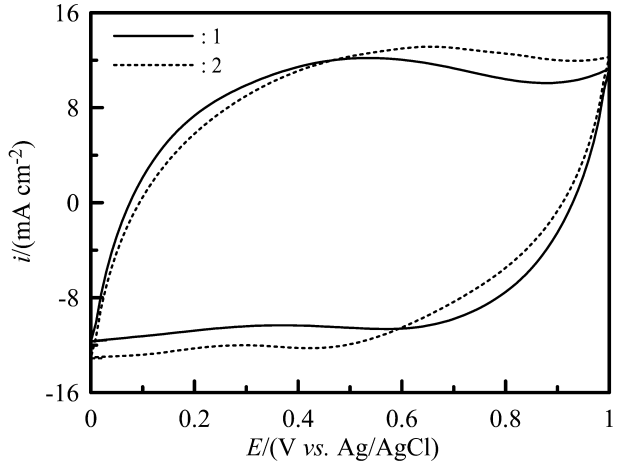

Fig. 7 Cyclic voltammograms of a-$MnO_x{\cdot}nH_2O$-3C and a-$MnO_x{\cdot}nH_2O$-3.5C measured in 0.1 M Na_2SO_4 at 25 mV s^{-1}

charges surrounded by curves 1 and 2 is small. This indicates that the energy capacity is slightly increased on increasing the oxide loading when the charge density of deposition is changed from 3 and 3.5 C cm^{-2}. Hence, the specific capacitance is, of course, lower for a-$MnO_x{\cdot}nH_2O$-3.5C without considering its relatively poorer reversibility. From the above results and discussion for Figs. 5, 6, and 7, a-$MnO_x{\cdot}nH_2O$-3.5C, showing acceptable capacitive performance, has the highest capacity for energy storage among all the a-$MnO_x{\cdot}nH_2O$ deposits.

The electrochemical reversibility of a-$MnO_x{\cdot}nH_2O$-3.5C was examined systematically by changing the upper potential limits of CV (see Fig. 8), since the electrochemical reversibility is the predominant factor influencing the power property of electrochemical supercapacitors. Note that the voltammetric currents gradually reach a plateau when the polarity of the potential sweeps is changed, indicating that the electrochemical reversibility of a-$MnO_x{\cdot}nH_2O$-3.5C is not as good as that of a-$MnO_x{\cdot}nH_2O$ with a lower charge density of deposition (e.g., 1.6 C cm^{-2}). However, the electrochemical reversibility of a-$MnO_x{\cdot}nH_2O$-3.5C is acceptable for the supercapacitor application. From a comparison of Figs. 5, 6, 7, and 8, the maximum of the voltammetric currents for various a-$MnO_x{\cdot}nH_2O$ deposits is close to 12.5 mA cm^{-2} at a scan rate of 25 mV s^{-1} in 0.1 M Na_2SO_4. Accordingly, a-$MnO_x{\cdot}nH_2O$-3.5C is proposed to be under the critical status with acceptable capacitive characteristics since the voltammetric currents of a-$MnO_x{\cdot}nH_2O$-3.5C reach the maximum.

Typical chronopotentiograms of the a-$MnO_x{\cdot}nH_2O$-3.5C deposit measured at ca. 1.0 and 2.5 A g^{-1} in 0.1 M Na_2SO_4 between 0 and 1.0 V are shown as curves 1 and 2 in Fig. 9, respectively. On both curves, the anodic charge parts are mirror-symmetrical to their corresponding cathodic discharge counterparts, although the *iR* drop becomes more significant on increasing the applied current densities when the polarity of applied currents is changed. In addition, the time period of one charge–discharge cycle reaches 450 and 165 s at 1 and 2.5 A g^{-1}, respectively, revealing the fact that the capacity of a-$MnO_x{\cdot}nH_2O$-3.5C is insignificantly affected by the current density of charge–discharge. Moreover, the stability of this electrode is excellent since the capacity loss is below 12% after 500 cycles of the charge–discharge test under the larger applied current density (i.e., 2.5 A g^{-1}). All these results reveal the excellent characteristics of a-$MnO_x{\cdot}nH_2O$-3.5C for application as supercapacitors in the operation potential window of ca. 1.0 V. Therefore, anodic deposition of a-$MnO_x{\cdot}nH_2O$ from $Mn(CH_3COO)_2{\cdot}4H_2O$ has been demonstrated to successfully fabricate a high-capacity electrode with excellent performance.

Based on curves 1 and 2 in Fig. 9, the average power density of this electrode is equal to 0.5 and 1.25 kW/kg, respectively, which can be estimated from the following equation:

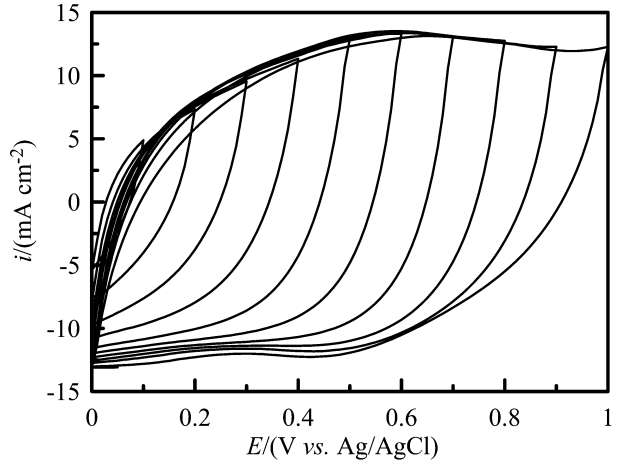

Fig. 8 Cyclic voltammograms of a-$MnO_x{\cdot}nH_2O$-3.5C with variation of the upper potential limit of CV in 0.1 M Na_2SO_4 at 25 mV s^{-1}

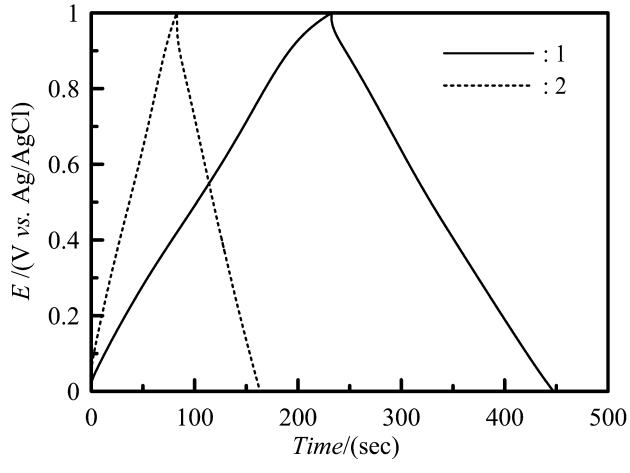

Fig. 9 Chronopotentiograms of a-$MnO_x{\cdot}nH_2O$-3.5C measured at *1* 1 and *2* 2.5 A g^{-1} in 0.1 M Na_2SO_4 between 0 and 1 V

$$P = \frac{E}{tw} = \frac{Q\Delta V}{2tw} \quad (3)$$

where P, E, t, w, Q, and ΔV are indicative of the average power density, total energy stored, discharge time, loading of a-$MnO_x{\cdot}nH_2O$-3.5C, total charges delivered, and the potential window of discharge, respectively. This fairly high-power density meets one of the basic requirements for an electrode material of supercapacitors [2].

From all the above results and discussion, as well as the ease of electrode fabrication and the cost of Mn precursors compared with other transition metal precursors, a-$MnO_x{\cdot}nH_2O$ prepared by anodic deposition from manganese acetate shows its commercial potential in the application of electrochemical supercapacitors.

Conclusions

The deposition rate of a-$MnO_x{\cdot}nH_2O$ from $Mn(CH_3COO)_2{\cdot}4H_2O$ was much faster than that from $MnSO_4{\cdot}5H_2O$, $MnCl_2{\cdot}4H_2O$, and $Mn(NO_3)_2{\cdot}4H_2O$ at 1.0 V. The capacitive characteristics of a-$MnO_x{\cdot}nH_2O$ were found to be independent of precursors, probably due to the amorphous and nonstoichiometric nature of all a-$MnO_x{\cdot}nH_2O$ deposits with a similar mean oxidation state of Mn, from the XRD and XPS results. The capacity of a-$MnO_x{\cdot}nH_2O$ was directly proportional to the loading of a-$MnO_x{\cdot}nH_2O$ when it was equal to or less than a critical value (ca. 2.5 mg cm^{-2}), while poorer capacitive behavior with a lower capacity was clearly found beyond this critical value. The a-$MnO_x{\cdot}nH_2O$ deposit with a deposition charge density of 3.5 C cm^{-2}, exhibiting an acceptable capacitive performance, exhibited the highest capacity of energy storage for supercapacitors. From the electrochemical results, the ease in electrode fabrication, and the cost of Mn precursors, a-$MnO_x{\cdot}nH_2O$ prepared by anodic deposition from $Mn(CH_3COO)_2{\cdot}4H_2O$ showed the commercial potential for electrochemical supercapacitors.

Acknowledgments The financial support of this work, by the National Science Council of the Republic of China under contract no. NSC 92-2214-E-194-005, is gratefully acknowledged.

References

1. Conway BE (1999) Electrochemical supercapacitors. Kluwer-Plenum, New York
2. Burke A (2000) J Power Sources 91:37
3. Zheng JP, Huang J, Jow TR (1997) J Electrochem Soc 144:2026
4. Hu C-C, Huang Y-H (1999) J Electrochem Soc 146:2465
5. Hu C-C, Chiang H-R, Wang C-C (2003) J Solid State Electrochem (in press)
6. Nomoto S, Nakata H, Yoshioka K, Yoshida A, Yoneda H (2001) J Power Sources 97–98:807
7. Bard AJ, Faulkner LR (1980) Electrochemical methods, fundamentals and applications. Wiley, Singapore
8. Hu C-C, Chang K-H (2000) Electrochim Acta 45:2685
9. Lee HY, Goodenough JB (1999) J Solid State Chem 148:81
10. Hu C-C, Chen C-Y (2002) Electrochem Solid-State Lett 5:A43
11. Hu C-C, Tsou T-W (2002) Electrochem Commun 4:105
12. Hu C-C, Lin X-X (2002) J Electrochem Soc 149:A1049
13. Hu C-C, Chu C-H (2001) J Electroanal Chem 503:105
14. Lee HY, Goodenough JB (1999) J Solid State Chem 144:220
15. Kim H, Popov BN (2003) J Electrochem Soc 150:D56
16. Pang S-C, Anderson MA, Chapman TW (2000) J Electrochem Soc 147:444
17. Hu C-C, Tsou T-W (2002) Electrochem Acta 47:3523
18. Hu C-C, Wang C-C (2003) J Electrochem Soc 150:A1079
19. Hu, C-C, Tsou T-W (2003) J Power Sources 115:179
20. Chen Y-S, Hu C-C (2003) Electrochem Solid-State Lett 6:A210
21. Chigane M, Ishikawa M (2000) J Electrochem Soc 147:2246
22. Chigane M, Ishikawa M, Izaki M (2001) J Electrochem Soc 148:D96